Metal Flux in Ligand Mixtures. 2. Flux Enhancement Due to Kinetic Interplay: Comparison of the Reaction Layer Approximation with a Rigorous Approach

Zeshi Zhang,*,† Jacques Buffle,† Raewyn M. Town,‡ Jaume Puy,§ and Herman P. van Leeuwen||

Analytical and Biophysical Environmental Chemistry (CABE), University of Geneva, Sciences II, 30 quai E. Ansermet, 1211 Geneva 4, Switzerland, Institute for Physics and Chemistry, University of Southern Denmark, Campusvej 55, DK5230 Odense, Denmark, Department of Chemistry, University of Lleida, Av. Rovira Roure 191, 25198 Lleida, Spain, and Laboratory of Physical Chemistry and Colloid Science, Wageningen University, Dreijenplein 6, NL-6703 HB, The Netherlands

Received: December 26, 2008; Revised Manuscript Received: February 26, 2009

The revisited reaction layer approximation (RLA) of metal flux at consuming interfaces in ligand mixtures, discussed in the previous paper (part 1 of this series[15]) is systematically validated by comparison with the results of rigorous numerical simulations. The current paper focuses on conditions under which the total metal flux is enhanced in the ligand (and complex) mixture compared to the case where the individual fluxes of metal complexes are independent of each other. Such an effect is exhibited only in ligand mixtures and results from the kinetic interplay between the various complexes with different labilities. It is exemplified by the Cu/NTA/*N*-(2-carboxyphenyl)glycine system (see part 1 paper), in which we show that the flux due to the less labile complex (CuNTA) is increased in the presence of a ligand (2-carboxyphenyl)glycine) that forms labile Cu complexes, even when the latter is in negligible proportion in the bulk solution. This paper first explains how the so-called composite and equivalent reaction layer thicknesses computed by RLA can be determined graphically from the concentration profiles of free metal and its complexes, as obtained by rigorous calculations. This approach allows comparison between the latter and RLA predictions. Comparison between these reaction layer thicknesses is then done using the chemical system mentioned above. The mechanism of flux enhancement with this system is studied in detail by following the change of the concentration profiles and reaction layer thicknesses with the increase of concentration of the ligand forming labile complexes. The mechanism of flux enhancement is well explained by the RLA and is validated by the concentration profiles obtained by rigorous numerical simulations. Based on this validation, the RLA is used to predict the conditions of the individual complex labilities and degree of complexation required to get flux enhancement in a two-ligand system. Due to compensation effects between kinetic and thermodynamic factors, a maximum flux enhancement is observed in a specific range of ratios of the lability indices of the two complexes. Flux enhancement might play a significant role in metal uptake in environmental or biological systems and should be considered in data interpretation.

1. Introduction

The bio-uptake of vital or toxic metals by microorganisms is frequently assumed to follow the free-ion activity model[1−3] or the biotic ligand model[3,4] in which all chemical species of a given metal are considered to be at equilibrium with each other in the exposure medium. The metal uptake is then only controlled by the free metal ion's activity (fixed by its thermodynamic speciation) and its transfer rate through the plasma membrane. However, in a number of cases,[3,5−8] particularly under conditions close to those of natural systems, such as microorganism starvation,[9] the dynamic processes, such as diffusion in solution or kinetics of interconversion of chemical species, may become the limiting factors for bio-uptake. The importance of dynamic metal speciation is increasingly recognized for understanding metal bio-availability and making predictions on dynamic risk assessment.[3,5,10,11]

We consider the case of an interfacial process in which a metal ion, M, is consumed in the presence of ligands forming metal complexes. The overall flux of M toward the interface results from the coupled diffusion and kinetics of interconversion between M and its various complexes. Recently, rigorous mathematical approaches have been derived for computing the metal flux at consuming interfaces in the presence of multiligand systems by solving the diffusion/reaction processes with either an analytical solution[12] or the numerical Lattice-Boltzmann method.[13,14] These new approaches make it possible to compute the exact values of the total flux as well as the individual contributions to the flux from each metal species. In particular, such computations have shown[15] that the total metal flux is unexpectedly enhanced when ligand forming labile complexes is added to a solution containing less labile complexes, even when the former is a practically negligible component of the bulk speciation. In other words, the ligand forming labile complexes plays a catalytic-type role in the metal flux. However, the intrinsic mathematical complexity of the above two rigorous

* Corresponding author: Present address: Department of Chemistry, University of Montreal, C. P. 6128, Succursale Centre-Ville, Montreal (QC), Canada, H3C 3J7. Telephone: ++1-514-3436111 (ext. 0698). E-mail: zeshi.zhang@umontreal.ca.

† University of Geneva.

‡ University of Southern Denmark.

§ University of Lleida.

|| Wageningen University.

10.1021/jp8114308 CCC: $40.75
Published on Web 05/21/2009

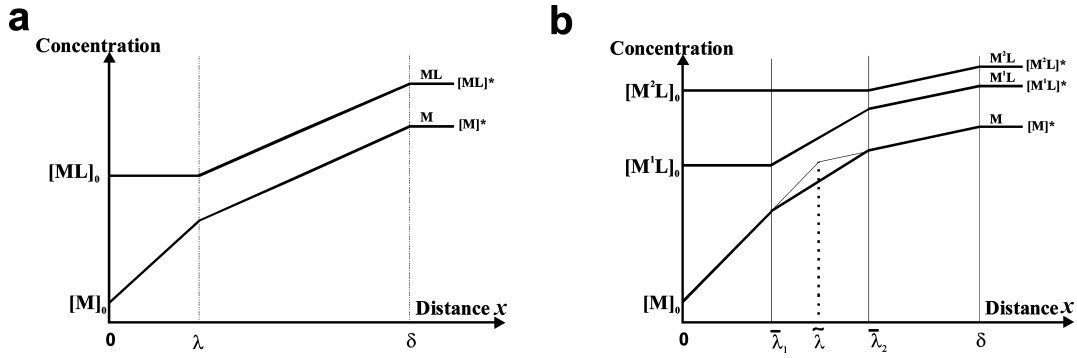

Figure 1. (a) Schematic view of the concentration profiles in a solution containing one ligand L and one complex ML. (b) Schematic concentration profiles of M, M^1L, and M^2L in a solution with two ligands, ^1L and ^2L, and two complexes, M^1L and M^2L, with different formation/dissociation rate constants. Under perfect sink condition (as in this paper), $[M]_0 = 0$.

approaches precludes a detailed physicochemical understanding of the mechanism of this flux enhancement.

Recently, it has been shown[15] that the flux enhancement in mixed ligand systems can be explained via the reaction layer concept,[16] which was initially developed by Brdička, Koutecký, and other members of the Heyrovský School,[16−21] for solutions containing one ligand, L, and one complex, ML (Figure 1a). This so-called Koutecký−Koryta (KK) approximation is based on the spatial division of the concentration profiles for M and ML in the diffusion layer, δ, into nonlabile ($0 \le x \le \lambda$) and labile regions ($\lambda \le x \le \delta$), separated by the boundary of the reaction layer with a thickness, λ (Figure 1a). (Note that μ is used instead of λ in refs 16−21; λ is just a more general mathematical expression.[15,24]) ML is assumed to be at equilibrium with M and L in $\lambda \le x \le \delta$. The flux due to dissociation of ML and diffusion of free M in the reaction layer ($0 < x < \lambda$) equals the diffusive flux of M + ML toward the reaction layer boundary ($\lambda < x < \delta$). In addition, in the reaction layer approximation (RLA) in $0 \le x \le \lambda$, the concentration of ML is considered as constant because ML is not consumed directly at the interface and its dissociation is weak compared to the diffusion flux of M. The reaction layer thickness, λ (or μ), is fixed by the competition between the re-association rate of free M (with L) and its diffusion rate, which enables it to reach the interface before re-association can occur.[15−21] The KK approximation has found wide application for computation of fluxes in a very simple, but, nevertheless, precise manner in the complete kinetic range from nonlabile to labile complexes for any metal-to-ligand ratio.[16,22] It also leads to a simple understanding of physicochemical processes of diffusion/reaction. For instance, the purely kinetic metal flux at a planar consuming interface (Figure 1a) can be computed either from the concentration gradient of free metal ion:

$$J = D_M\left(\frac{d[M]}{dx}\right)_{x=0} = D_M\frac{[M]_\lambda}{\lambda} \quad (1)$$

(assuming $[M]_0 = 0$), or from the chemical dissociation of ML inside the reaction layer:

$$J = k_d[ML]_0\lambda \quad (2)$$

where $[ML]_0 = [ML]_{x=0}$ and k_d is the dissociation rate constant of ML.

This concept has been extended to multiligand systems,[15,23] at either planar or spherical consuming interfaces. In such a system, a series of so-called composite reaction layers ($\bar{\lambda}_1$, $\bar{\lambda}_2$...; Figure 1b) are defined for each of the metal complexes (M^1L, M^2L,...) formed with the ligands ^1L, ^2L... In mixtures, the reaction layer of a given complex is called "composite" because it depends primarily on the rate constants of formation/dissociation of the pertinent complex, but it is also dependent on the complexation and diffusion properties of the other complexes present. It has also been shown[15] that, analogous to the single complex case, the metal flux in a ligand mixture can be computed based on a single "equivalent" reaction layer, $\tilde{\lambda}$, which is a combination of the various composite layers (Figure 1b; see also Definitions and Symbols for definitions of the various reaction layer thicknesses). This approach is called the reaction layer approximation (RLA). It has been used to explain the physicochemical basis for the above-mentioned unexpected flux enhancement:[15] the latter results from the thermodynamic buffering of the free metal ion concentration at $x = \tilde{\lambda}$ combined with a decrease in $\tilde{\lambda}$ when the concentration of the ligand forming labile complexes increases. As a consequence, J ($= D_M(d[M]/dx)_{x=0} = D_M[M]_{\tilde{\lambda}}/\tilde{\lambda}$) increases (Figure 1b).

The purpose of this paper is two-fold:

(1) We shall validate the equations derived for the composite reaction layer thicknesses in ligand mixtures[15] by comparing them with the concentration profiles of free and complexed metal species computed by rigorous mathematical solutions. For the sake of clarity, this will be done for a two-ligand system by using, as an example, the system Cu/NTA/*N*-(2-carboxyphenyl)glycine, which exhibits flux enhancement.[15]

(2) Based on this validation, we will determine the conditions under which a flux enhancement can be observed in a two-ligand system. These conditions are deduced from contour plots of the flux enhancement for variable values of the lability indices of each complex (as arising from changes in [L] or K), which, in turn, are directly related to the thickness of the corresponding reaction layers.

2. Theory

In this paper, concentration profiles of M, M^1L, and M^2L and the corresponding individual fluxes are computed rigorously by using the computer code MHEDYN (Multispecies HEtergeneous DYNamics, see Computation Method section). To demonstrate the validity of the RLA in ligand mixtures, the fluxes and composite reaction layer thicknesses of M^1L and M^2L computed by the RLA[15] are compared to those obtained from the rigorous concentration profiles. Below, we show how the composite reaction layers can be obtained graphically from these rigorous concentration profiles.

2.1. Finding the Reaction Layer Thickness from Plots of Concentration Profiles. To find reaction layer thicknesses in a two-ligand system, it is easier to look first at a one-ligand system (Figure 2a). Figure 2a shows, for an excess of L and at

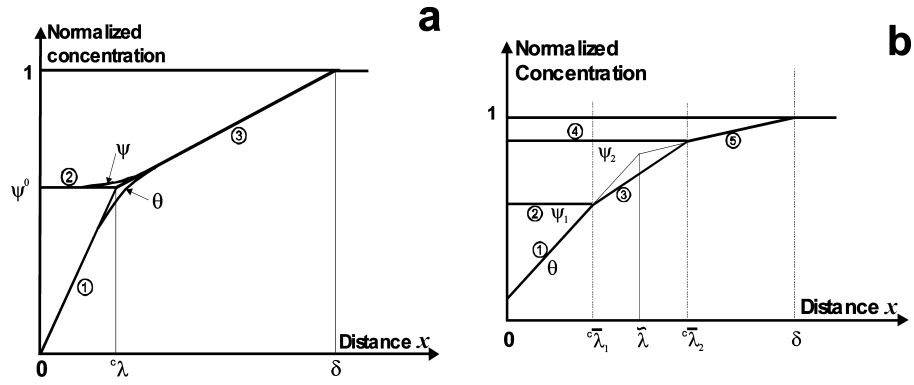

Figure 2. (a) Schematic view of the normalized concentration profiles in a solution with one ligand and one complex (when $\theta_0 = [M]_0 = 0$). (b) Schematic normalized concentration profiles of M, M^1L, and M^2L in a solution with two ligands, ^1L and ^2L, and two complexes, M^1L and M^2L, with different formation/dissociation rate constants.

steady-state, the rigorous normalized concentration profiles of M, $\theta = [M]/[M]^*$, and ML, $\psi = [ML]/[ML]^*$, where $[M]^*$ and $[ML]^*$ denote the bulk concentrations of M and ML, respectively. Figure 2a also shows the straight lines (1 and 3) and (2 and 3), which are the profiles of θ and ψ, respectively, assumed in the RLA. These lines are the tangent of $\theta(x)$ at point ($x = 0$, $y = 0$) (line 1), the tangent of $\psi(x)$ at point ($x = 0$, $y = \psi_0$) (line 2), and the tangent of $\psi(x)$ at point ($x = \delta$, $y = 1$) (line 3). Below, we show that, in practice, the reaction layer thickness can be found on the x-axis at the intersection of any two of these three lines.

The functions $\theta(x)$ and $\psi(x)$ are[15,24]

$$\theta = C_1 \exp(-x/\lambda) + C_2 \exp(x/\lambda) + \frac{\left(\frac{d\theta}{dx}\right)_{x=0} x}{1 + \varepsilon K[L]} + 1 - \frac{\left(\frac{d\theta}{dx}\right)_{x=0} \delta}{1 + \varepsilon K[L]} \quad (3)$$

$$\psi = \frac{C_1}{\varepsilon K[L]} \exp(-x/\lambda) + \frac{C_2}{\varepsilon K[L]} \exp(x/\lambda) + \frac{\left(\frac{d\theta}{dx}\right)_{x=0} x}{1 + \varepsilon K[L]} + 1 - \frac{\left(\frac{d\theta}{dx}\right)_{x=0} \delta}{1 + \varepsilon K[L]} \quad (4)$$

with

$$C_1 = \frac{1}{2}\left(\frac{\left(\frac{d\theta}{dx}\right)_{x=0} \delta}{1 + \varepsilon K[L]} - 1\right) \exp\left(\frac{\delta}{\lambda}\right) \operatorname{csch}\left(\frac{\delta}{\lambda}\right)$$

$$C_2 = \frac{1}{2}\left(1 - \frac{\left(\frac{d\theta}{dx}\right)_{x=0} \delta}{1 + \varepsilon K[L]}\right) \exp\left(-\frac{\delta}{\lambda}\right) \operatorname{csch}\left(\frac{\delta}{\lambda}\right)$$

$$\lambda = \sqrt{\frac{D_M}{k_a[L] + k_d/\varepsilon}} = \sqrt{\frac{D_{ML}/k_d}{1 + \varepsilon K[L]}} \quad (5)$$

where k_a and k_d are the association and dissociation rate constants, respectively, $\varepsilon = D_{ML}/D_M$ is the ratio of the diffusion coefficients of the complex ML, and free metal ion M, csch(x) is the hyperbolic cosecant of x, δ is the diffusion layer thickness, K is the stability constant of ML, [L] is the ligand concentration, and λ is the reaction layer thickness of ML in a solution containing only one ligand, L, when the diffusion domain is infinite.[15,24] As explained in ref 24, λ is a more general expression of the reaction layer thickness than the conventional one ($\mu = (D_M/k_a[L])^{1/2}$), which is valid only when $\varepsilon K[L] \gg 1$.

From eq 3, the normalized concentration profile for the free M at $x = 0$ follows as

$$\left(\frac{d\theta}{dx}\right)_{x=0} = \left(\frac{\delta}{1 + \varepsilon K[L]} + \frac{\lambda \varepsilon K[L]}{1 + \varepsilon K[L]} \tanh\left(\frac{\delta}{\lambda}\right)\right)^{-1} \quad (6)$$

while the surface-normalized concentration of ML derived from eq 4 is:

$$\psi^0 = \frac{\lambda \tanh\left(\frac{\delta}{\lambda}\right)(1 + \varepsilon K[L])}{\delta + \lambda \varepsilon K[L] \tanh\left(\frac{\delta}{\lambda}\right)} \quad (7)$$

and it can be shown that when $\lambda \ll \delta$:

$$\left(\frac{d\psi}{dx}\right)_{x=\delta} = \frac{1}{\delta + \lambda \varepsilon K[L] \tanh\left(\frac{\delta}{\lambda}\right)} \quad (8)$$

Now from the slope of line 3 (Figure 2a) it follows

$$\psi^0 - 1 = \left(\frac{d\psi}{dx}\right)_{x=\delta} (x_i - \delta) \quad (9)$$

where x_i is the abcissa corresponding to the intersection of lines 2 and 3. By combining eqs 7−9, one gets

$$x_i = {}^c\lambda = \lambda \tanh\left(\frac{\delta}{\lambda}\right) \quad (10)$$

which indeed is the "effective" reaction layer thickness. As explained in ref 15, λ is the value of the reaction layer thickness under the condition of semi-infinite diffusion ($\delta \to \infty$). When a finite value is imposed to δ, the reaction layer cannot be larger than this value and the effective reaction layer thickness is corrected by the tanh term (for $\delta/\lambda > 3$, $\tanh(\delta/\lambda) \approx 1$, and ${}^c\lambda = \lambda$; for $0 < \delta/\lambda < 0.01$, $\tanh(\delta/\lambda) \approx \delta/\lambda$).

Similarly, the equation of line 1 (Figure 2a) is $\theta = (d\theta/dx)_{x=0} x$. In combination with eq 6 and $\theta = \psi^0$ (eq 7), we obtain the corresponding abscissa, x_i, of the intersection between lines 1 and 2:

$$x_i = {}^c\lambda \quad (11)$$

which shows that x_i is also equal to the corrected reaction layer thickness, ${}^c\lambda$ (eq 10). Thus, the intersection of any two of the lines 1, 2, or 3 of Figure 2a, as defined above, can indeed provide the reaction layer thickness. This provides three methods for finding ${}^c\lambda$.

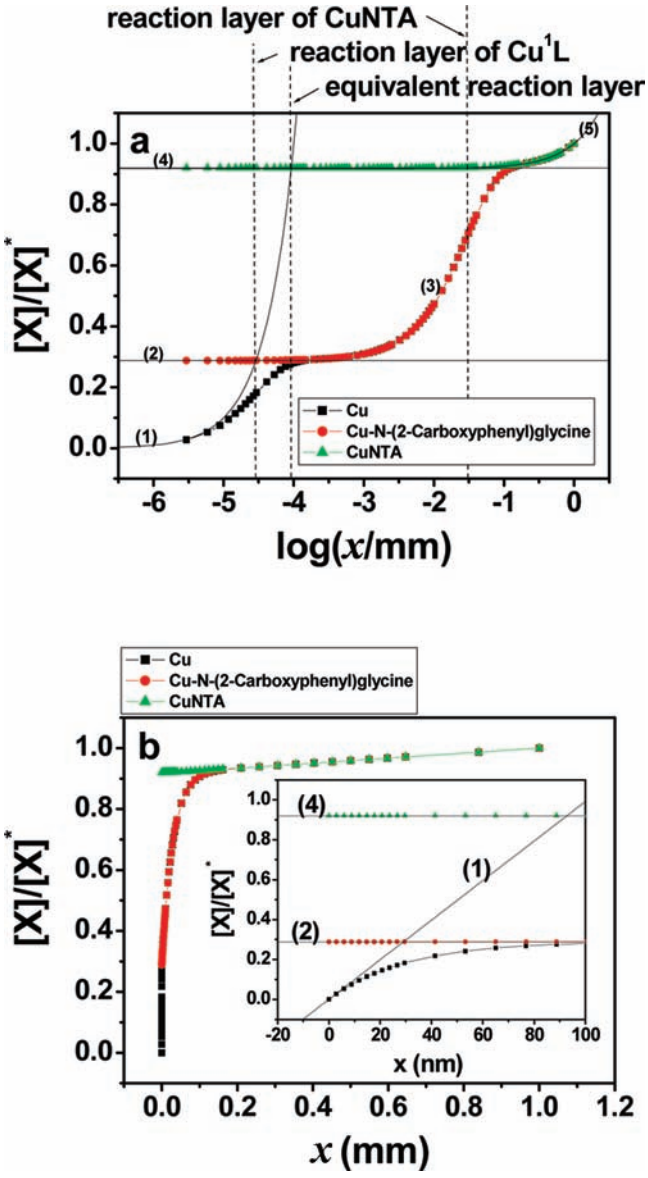

Figure 3. Normalized concentration profiles of Cu, CuNTA (≡Cu^2L), and Cu−*N*-(2-carboxyphenyl)glycine (≡Cu^1L) at [^{1}L] = 0.1 mM, [NTA] = 10^{-5} M, $[Cu]_t = 10^{-8}$ M, pH = 7.00, T = 25 °C, I = 0.1 M: (a) logarithmic plot and (b) linear plot. The solid lines correspond to the tangents at curves $\theta(x)$ (at points (0,0)), $\psi_1(x)$ (at point (0, $[CuL]_0/[CuL]^*$)), $\psi_2(x)$ (at point (0, $[CuNTA]_0/[CuNTA]^*$)), and $\psi_2(x)$ (at point (δ, 1)) in the linear plots. The numbers on the curves have the same meaning as in Figure 2b. Parameters: see Supporting Information, Table S1.

By extrapolating the above reasoning to a two-ligand system and making use of the above three combinations of intersections of lines, the following strategy can be adopted for the two-ligand system (Figure 2b).

(a) The intersection of lines 4 and 5 should be used for finding the reaction layer thickness, ${}^c\bar{\lambda}_2$, of the less labile complex, M^2L.

(b) The intersection of lines 1 and 2 should be used for finding the reaction layer thickness, ${}^c\bar{\lambda}_1$, of the more labile complex, M^1L. Indeed, the composite reaction layer of the more labile complex is always smaller than that of the less labile one.[15]

(c) The intersection of lines 1 and 5 should be used for finding the equivalent reaction layer thickness.

${}^c\bar{\lambda}_1$ and ${}^c\bar{\lambda}_2$ are the effective (corrected) composite reaction layers, given in ref 15. For a two-ligand system, the equivalent reaction layer (see above and ref 15) is given by:

$$\tilde{\lambda} = \frac{\alpha_t' - 1}{\alpha_t'}\left[{}^c\bar{\lambda}_1\left(1 - \frac{1}{\alpha_1'}\right) + {}^c\bar{\lambda}_2\left(\frac{1}{\alpha_1'} - \frac{1}{\alpha_t'}\right)\right] \quad (12)$$

with

$$\alpha_t' = 1 + {}^1\varepsilon^1 K[{}^1L] + {}^2\varepsilon^2 K[{}^2L],\ \alpha_1' = 1 + {}^1\varepsilon^1 K[{}^1L],\ \text{and}\ \alpha_2' = 1 + {}^2\varepsilon^2 K[{}^2L]$$

2.2. Fluxes and Flux Enhancement in Two-Ligand Systems. Since M^1L and M^2L are not consumed at the interface, the total flux of M, J_t, is rigorously expressed by eq 1, which in the frame of RLA reduces to

$$J_t = D_M[M]^*_{{}^c\bar{\lambda}_1}/{}^c\bar{\lambda}_1 \quad (13)$$

or equivalently:[15]

$$J_t = D_M[M]^*_{\tilde{\lambda}}/\tilde{\lambda} \quad (14)$$

It has been shown that the above equation can also be written as:[15]

$$J_t = \frac{J_{lab}}{1 + \dfrac{\tilde{\lambda}(\alpha_t' - 1)}{\delta}} \quad (15)$$

where J_{lab} is the maximum flux when all the complexes are fully labile (for definition of lability, see eq 20) and is equal to[15,16]

$$J_{lab} = \frac{D_M \alpha_t'[M]^*}{\delta} \quad (16)$$

Equations 14 and 15 take into account any possible interplay between M^1L and M^2L, which may lead to flux enhancement. If this interplay did not exist, then the total flux J_t^0 would simply be the sum of the separate fluxes of M, M^1L, and M^2L in the absence of the others, i.e.:

$$J_t^0 = J_M + J_{M^1L} + J_{M^2L} = \frac{J_{lab}}{\alpha_t'} + \frac{\dfrac{J_{lab}}{\alpha_t'}(\alpha_1' - 1)}{1 + \dfrac{{}^c\lambda_1(\alpha_1' - 1)}{\delta}} + \frac{\dfrac{J_{lab}}{\alpha_t'}(\alpha_2' - 1)}{1 + \dfrac{{}^c\lambda_2(\alpha_2' - 1)}{\delta}} \quad (17)$$

where ${}^c\lambda_1$ and ${}^c\lambda_2$ are the corrected reaction layer thicknesses in solution containing M and only ^{1}L or ^{2}L.

Accordingly, the flux enhancement factor is defined as

$$\sigma = \frac{J_t}{J_t^0} \quad (18)$$

Consider a solution containing both ^{1}L and ^{2}L and a constant total concentration of M, with M^1L being more labile than M^2L. When [^{1}L] increases (at a fixed concentration of ^{2}L), both J_t and J_t^0 may increase due to the increased proportion of the more labile M^1L. In such a case, however, σ remains equal to 1. A flux enhancement ($\sigma > 1$) only occurs when conditions are such that the lifetime of M at the interface is decreased (by formation of the labile complex M^1L), while its free concentration is maintained constant (by buffering with M^2L). These conditions are fulfilled when

(1) $[M]^* \ll [M^1L]^* \ll [M^2L]^*$, which also corresponds to $1 \ll \alpha'_1 \ll \alpha'_2$ for "simple ligands" for which $D_{ML} \approx D_M$ ($^1\varepsilon \approx {}^2\varepsilon \approx 1$), and

(2) M^1L is more labile than M^2L, i.e., ${}^c\lambda_1 \ll {}^c\lambda_2$.

It can be shown (Supporting Information, Section 1) that under these conditions, a flux enhancement ($\sigma > 1$) is observed when

$$\mathscr{L}_1 > \frac{1}{\sqrt{\alpha'_1}}\frac{{}^c\lambda_2}{{}^c\lambda_1} + \frac{{}^c\lambda_1}{{}^c\lambda_2} \qquad (19)$$

where $\mathscr{L}_1$ is the lability index of M^1L in the absence of ligand ^2L, given by[26]

$$\mathscr{L}_1 = \frac{\delta}{{}^c\lambda_1\,{}^1\varepsilon^1 K[{}^1L]} \approx \frac{\delta}{{}^c\lambda_1\alpha'_1} \qquad (20)$$

Note that ${}^c\lambda_1$ also includes $[^1L]$ (eq 5). The lability index is a useful composite parameter to classify quantitatively the lability of complexes: when $\mathscr{L} \gg 1$, the complexes are fully labile, i.e., they can dissociate and form again many times during their diffusion toward the consuming interface; when $\mathscr{L} \ll 1$, the complex is nonlabile, and the flux is controlled by its dissociation rate; when $10 > \mathscr{L} > 0.1$, the complex is semilabile.

3. Computation Method

The flux and concentration profiles are rigorously computed by using the flux computation code MHEDYN,[25] which is based on a Lattice-Boltzmann method for the numerical solution of the diffusion/reaction equations. It is coupled to a time splitting technique and a grid refinement method[13,14] in order to treat physicochemical systems with dynamic parameters varying over many orders of magnitude. Systems containing an unlimited number of ligands and complexes can be treated. MHEDYN allows the contribution to the metal flux and concentration profile of any species to be computed in the transient- and steady-state regimes, without requirement of ligand excess compared to metal. The boundary conditions used here are a planar consuming interface working as a perfect sink. At very small distances from the interface ($x < 10$ nm), the computation of precise concentration profiles may be very time consuming with MHEDYN. In this case, the equations derived in ref 12 have been used. The reaction layer thicknesses are computed based on the equations derived in the RLA.[15]

The rigorous contour plots (Figures 7 and 8, see below) are computed by the code FLUXY in its RS mode.[23,26] This algorithm is based on the rigorous analytical solution of diffusion/reaction equations[12] for conditions of excess ligand over metal. The computations with FLUXY are fast. User-friendly versions of MHEDYN and FLUXY codes are available at http://www.unige.ch/cabe/dynamic.

4. Results and Discussion

4.1. Reaction Layer Thicknesses: Comparison between RLA and Rigorous Concentration Profile Computations. Figure 3 shows examples of normalized concentration profiles of Cu, CuNTA, and Cu−*N*-(2-carboxyphenyl)glycine at 0.1 mM *N*-(2-carboxyphenyl)glycine. The composite reaction layer thicknesses and the equivalent reaction layer thicknesses indicated in Figure 3 are obtained by the method described in section 2.1. It can be seen that the reaction layer thickness of the less labile complex, CuNTA, is indeed the largest and that of Cu−*N*-(2-carboxyphenyl)glycine is the smallest, while the equivalent reaction layer thickness lies in between. The comparison of the reaction layer thicknesses determined from the concentration profiles with those computed by the RLA at different *N*-(2-carboxyphenyl)glycine concentrations is shown in Table 1. It can be seen that the values of reaction layer thicknesses of CuNTA determined by these two methods are very close to each other for all concentrations of *N*-(2-carboxyphenyl)glycine. The differences observed for ${}^c\lambda_1$ at small concentrations of *N*-(2-carboxyphenyl)glycine are somewhat larger, but still less than 25%. Part of this error may be due to the graphical uncertainties in plotting the tangent. In any case, the total flux in a ligand mixture computed via the equivalent reaction layer thickness never differs by more than a few percent from that computed rigorously.

TABLE 1: Reaction Layer Thicknesses Computed from the Concentration Profiles Obtained by Rigorous Computations and by the RLA[a]

	${}^c\bar{\lambda}_1$ (m)		${}^c\bar{\lambda}_2$ (m)		$\tilde{\lambda}$(m)	
log([^{1}L]/M)	RLA	from profile	RLA	from profile	RLA	from profile
−7.00	4.86e-07	3.90e-07	1.65e-06	1.51e-06	1.29e-06	1.25e-06
−6.30	3.37e-07	2.99e-07	2.47e-06	2.32e-06	9.96e-07	9.56e-07
−6.00	2.62e-07	2.43e-07	3.21e-06	2.83e-06	8.01e-07	7.77e-07
−5.30	1.29e-07	1.26e-07	6.63e-06	6.92e-06	4.07e-07	4.02e-07
−5.00	9.23e-08	9.09e-08	9.28e-06	9.35e-06	2.93e-07	2.90e-07
−4.30	4.17e-08	4.12e-08	2.06e-05	2.04e-05	1.33e-07	1.31e-07
−4.00	2.95e-08	2.90e-08	2.90e-05	2.86e-05	9.40e-08	9.25e-08

[a] ^{1}L is *N*-(2-carboxyphenyl)glycine and ^{2}L is NTA. yex = y10^x

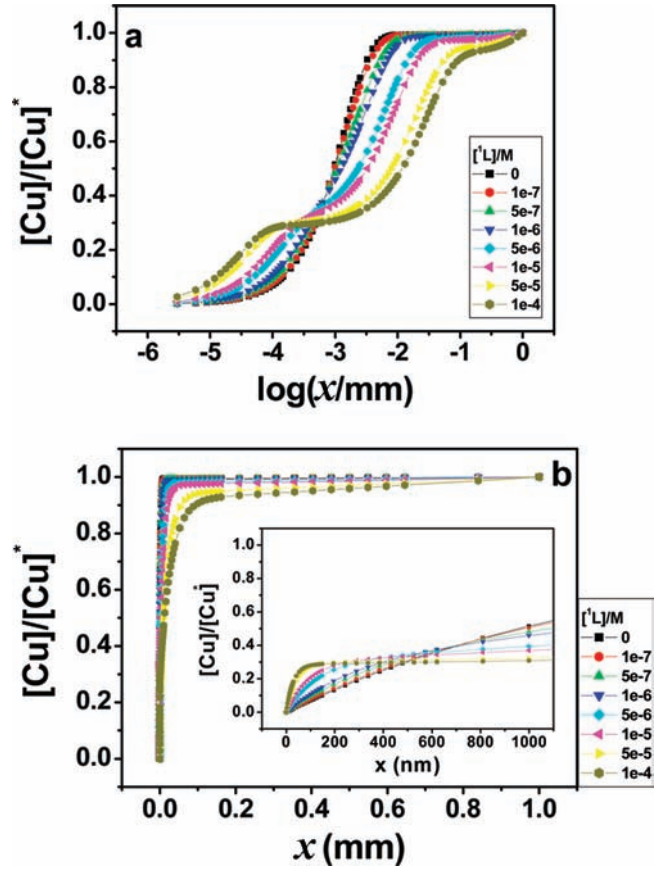

Figure 4. Normalized concentration profiles of free Cu at different concentrations of ^{1}L (*N*-(2-carboxyphenyl)glycine): (a) Logarithmic plot and (b) Linear plots (inset shows a different scale of *x*). [X]* is the bulk concentration of X. Parameters: see Supporting Information, Table S1. Boxes show concentrations of ^{1}L.

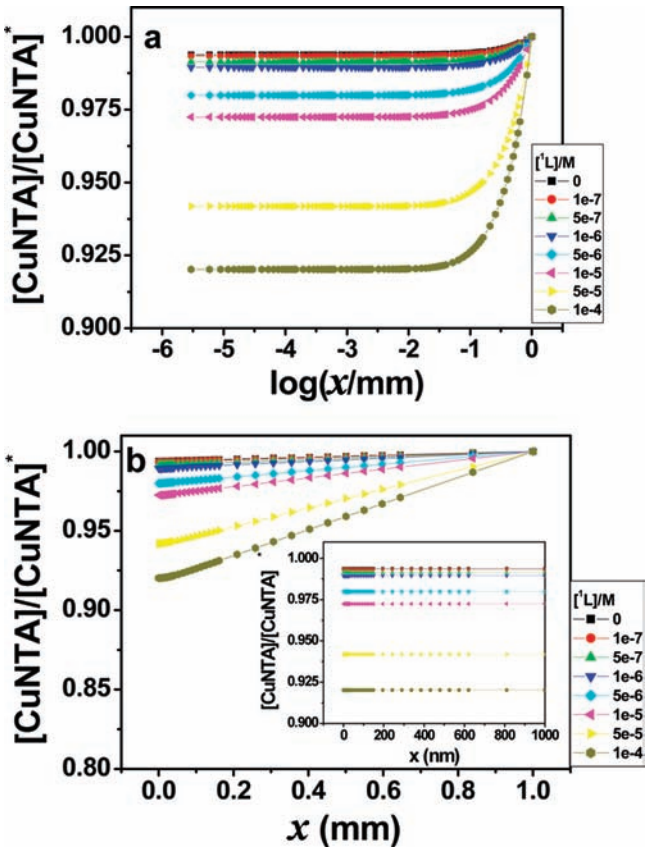

Figure 5. Normalized concentration profiles of CuNTA at different concentrations of ^{1}L(*N*-(2-carboxyphenyl)glycine): (a) Logarithmic plot and (b) Linear plots (inset shows a different scale of x). [X]* is the bulk concentration of X. Parameters: see Supporting Information, Table S1. Boxes show concentrations of ^{1}L.

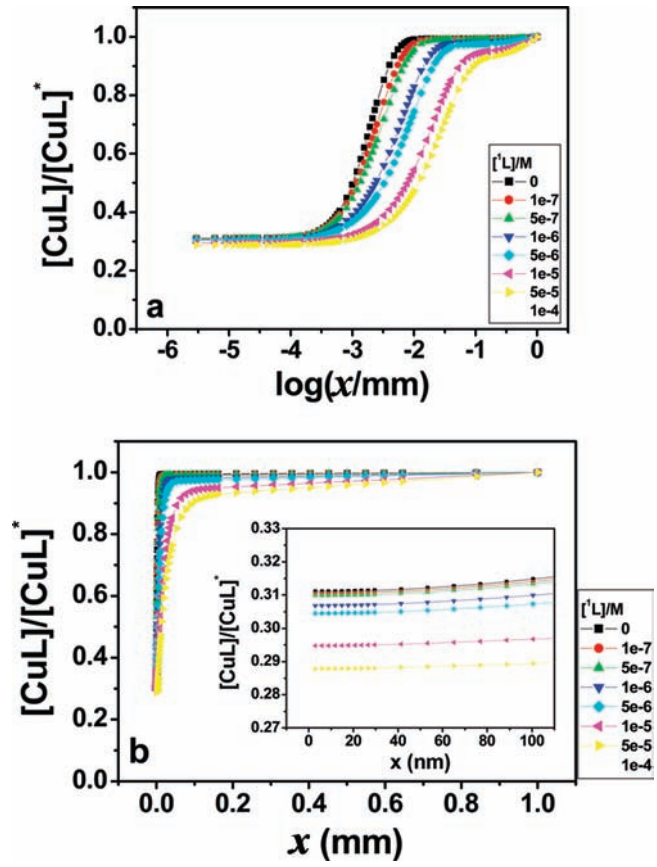

Figure 6. Normalized concentration profiles of Cu^{1}L at different concentrations of ^{1}L (*N*-(2-carboxyphenyl)glycine): (a) Logarithmic plot and (b) Linear plot (inset shows a different scale of x). [X]* is the bulk concentration of X. Parameters: see Supporting Information, Table S1. Boxes show concentrations of ^{1}L.

4.2. Flux Enhancement: Comparison between RLA and Rigorous Computations. Figures 4−6 show the normalized concentration profiles of Cu, CuNTA (≡Cu^{2}L), and Cu−*N*-(2-carboxyphenyl)glycine (≡Cu^{1}L), at different *N*-(2-carboxyphenyl)glycine concentrations. It can be seen that for free Cu (Figure 4), the concentration gradient at $x = 0$ increases with the concentration of *N*-(2-carboxyphenyl)glycine, which reflects a corresponding increase of the total flux. The normalized concentration of free Cu at the boundary of the composite reaction layer of Cu−*N*-(2-carboxyphenyl)glycine, $^c\bar{\lambda}_1$ (Table 2), is almost constant, and the same trend is observed at the boundary of the equivalent reaction layer, $\tilde{\lambda}$, because [Cu] is buffered by NTA over the whole range of *N*-(2-carboxyphenyl)glycine concentrations (Supporting Information, Figure S1). On the other hand, $^c\bar{\lambda}_1$ decreases from 3.90×10^{-7} m (based on concentration profiles; 4.86×10^{-7} m based on RLA) to 2.90×10^{-8} m (from concentration profiles; 2.95×10^{-8} m from RLA) when the concentration of *N*-(2-carboxyphenyl)glycine increases (Table 1). Interestingly, the equivalent reaction layer, $\tilde{\lambda}$, follows the same trend as $^c\bar{\lambda}_1$ (a decrease by a factor of ∼10 when [^{1}L] increases), while simultaneously $^c\bar{\lambda}_2$ increases. Thus, $\tilde{\lambda}$ is controlled by the kinetics of the more labile complex, Cu^{1}L, even when its bulk concentration is negligible compared to Cu^{2}L.

The constant value of $[Cu]_{^c\bar{\lambda}_1}$ combined with the decreasing value of $^c\bar{\lambda}_1$ when [^{1}L] increases leads to the corresponding increase of the total flux, J_t, (Table 2) computed by eq 13 based on $^c\bar{\lambda}_1$. Because the changes of the values of $[Cu]_{\tilde{\lambda}}$ and $\tilde{\lambda}$ closely follow those of $[Cu]_{^c\bar{\lambda}_1}$ and $^c\bar{\lambda}_1$, respectively, the values of J_t obtained from the RLA[15] (eq 15 based on $\tilde{\lambda}$) are very close to the rigorous ones.

The normalized surface concentrations of Cu−*N*-(2-carboxyphenyl)glycine ([Cu^{1}L], Figure 6) are almost constant over the whole range of *N*-(2-carboxyphenyl)glycine concentration. This shows that its degree of lability ($\xi_1 = 1 - [Cu^1L]_0/[Cu^1L]^*$) remains almost constant, irrespective of [^{1}L]. Thus, the flux enhancement cannot be explained by a contribution of Cu−*N*-(2-carboxyphenyl)glycine, by an increase of either its degree of lability or bulk concentration, since the latter is always negligible in the whole range of [^{1}L] (Supporting Information, Figure S1).

The normalized concentrations of CuNTA (Figure 5) at the consuming surface decrease from 0.99373 (for [^{1}L] = 0) to 0.92925 ([^{1}L] = 0.1 mM), which results in a 10-fold increase in its degree of lability, from 0.00627 to 0.06075. Thus, CuNTA becomes more labile in the presence of Cu−*N*-(2-carboxyphenyl)glycine. Since the degree of complexation of CuNTA is much larger than that of Cu^{1}L, [Cu] is well buffered by CuNTA, and its bulk concentration is constant in the whole range of *N*-(2-carboxyphenyl)glycine concentration (Supporting Information, Figure S1). The net effect is that the individual flux due to CuNTA increases about 10-fold because of the corresponding increase of its lability degree, which results in the observed flux enhancement.

4.3. Conditions for Flux Enhancement in Two-Ligand Systems. In this section we discuss the conditions under which a significant flux enhancement ($\sigma > 1$) can be observed. Even with a system including only two ligands and two complexes,

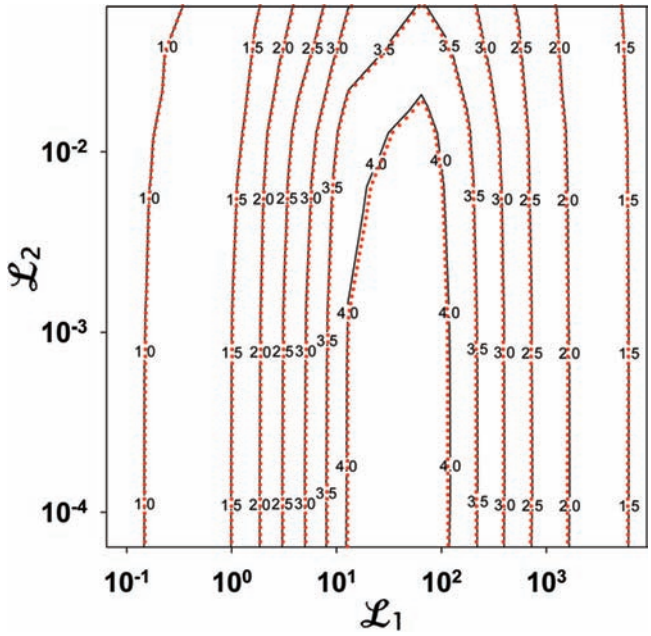

Figure 7. Contour plot of the flux enhancement as a function of lability indices of two complexes by changing their stability constants. Black solid line is the rigorous solution. Red dotted line is the RLA. Parameters: see Supporting Information, Table S2.

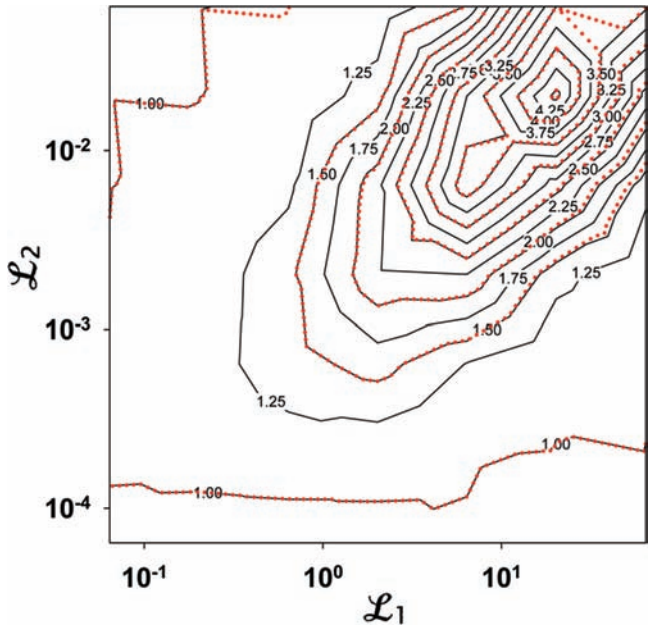

Figure 8. Contour plot of the flux enhancement as a function of lability indices of two complexes by changing ligand concentrations. Black solid line is the rigorous solution. Red dotted line is the RLA. Parameters: see Supporting Information, Table S3.

σ may be influenced by up to 10 independent parameters (four rate constants, three diffusion coefficients, one δ value, and two ligand concentrations). Thus, it is not a simple task to describe the optimum conditions under which $\sigma > 1$. As discussed in section 2.2 and the Supporting Information, an approximate condition (eq 19) relates $\mathcal{L}_1$ to α'_1, ${}^c\lambda_1$, and ${}^c\lambda_2$. In the following, we study these optimum conditions by means of contour plots of σ values as a function of the individual lability indices, $\mathcal{L}_1$ and $\mathcal{L}_2$, of M^1L and M^2L; $\mathcal{L}$ is a good combination parameter which is sensitive to the whole of the dynamic properties of a given complex. Nevertheless, σ is not a function of $\mathcal{L}_1$ and $\mathcal{L}_2$ only. Thus, different contour plots can be obtained (e.g., Figure 7 and 8) depending on which parameters are varied to change the values of $\mathcal{L}_1$ and $\mathcal{L}_2$.

TABLE 2: Normalized Free Cu Concentrations (i) at the Boundary of the Effective Composite Reaction Layer, ${}^c\bar{\lambda}_1$, of Cu^1L Computed from the Concentration Profiles and from the RLA, and (ii) at the Boundary of the Equivalent Reaction Layer, $\tilde{\lambda}$, (see also Table 1)[a]

	$[Cu]_{{}^c\bar{\lambda}_1}/[Cu]^*$			J_t/J_t^0	
log([^{1}L]/M)	${}^c\bar{\lambda}_1$ from RLA	${}^c\bar{\lambda}_1$ from profiles	$[Cu]_{\tilde{\lambda}}/[Cu]^*$	RLA	rigorous computation
−7.00	0.30	0.25	0.993	1.06	1.09
−6.30	0.25	0.23	0.991	1.38	1.40
−6.00	0.23	0.22	0.989	1.69	1.71
−5.30	0.20	0.20	0.980	3.17	3.18
−5.00	0.20	0.19	0.972	4.23	4.22
−4.30	0.19	0.19	0.941	7.32	7.30
−4.00	0.18	0.18	0.919	8.23	8.23

[a] ^{1}L is *N*-(2-carboxyphenyl)glycine.

Figure 7 shows contour plots of the flux enhancement factor, σ (eq 18), as a function of $\mathcal{L}_1$ and $\mathcal{L}_2$ when their values are changed via variation of the stability constants, ${}^1K$ and ${}^2K$. The predictions of flux enhancement by the RLA (red dotted line) are almost the same as those obtained by the rigorous analytical solutions.[12] Both methods predict that by varying ${}^1K$ and ${}^2K$, σ is almost independent of $\mathcal{L}_2$ in most of the plot and that the maximum value of σ is found at $\mathcal{L}_1 \approx 70$. The contour plot also shows that, when M^1L and M^2L have the same lability indices ($\mathcal{L}_2 = \mathcal{L}_1$), $\sigma \approx 1$ (the upper left corner of Figure 7).

The fact that σ is almost independent of $\mathcal{L}_2$ when ${}^1K$ is constant and ${}^2K$ decreases can be explained by the RLA, as follows. By combining eqs 15 and 17 with $J_M \ll J_{M^1L}$ and $J_M \ll J_{M^2L}$, we find that

$$\sigma = \left(\frac{1}{\frac{\delta}{\alpha'_1} + {}^c\lambda_1} + \frac{1}{\frac{\delta}{\alpha'_2} + {}^c\lambda_2}\right)^{-1}\left(\frac{1}{\frac{\delta}{\alpha'_t} + \tilde{\lambda}}\right) \qquad (21)$$

which can also be written as:

$$\sigma = \frac{\left(\frac{\alpha'_t/\delta}{1 + \tilde{\lambda}\alpha'_t/\delta}\right)}{\left(\frac{\alpha'_1/\delta}{1 + 1/\mathcal{L}_1} + \frac{\alpha'_2/\delta}{1 + 1/\mathcal{L}_2}\right)} \qquad (21a)$$

Since $\mathcal{L}_2 \ll 1$, $1/\mathcal{L}_2 \gg 1$ and the second term in the denominator is equal to ${}^c\bar{\lambda}_2$ which is independent of ${}^2K$. Thus, the whole denominator of eq 21a is constant when ^{2}K varies. In addition, $\tilde{\lambda}$ is almost independent of ${}^2K$, under the condition $\alpha'_t \gg 1$ (eq 12), which was used to draw Figure 7 (section 2.2). Thus, both the numerator and denominator of eq 21a are almost independent of ${}^2K$.

Figure 8 shows the contour plots obtained by varying $\mathcal{L}_1$ and $\mathcal{L}_2$ via changes in the ligand concentrations [^{1}L] and [^{2}L]. This case is a bit more complicated than the former one because varying the ligand concentration changes not only the degree of complexation, but also changes the ${}^c\bar{\lambda}$ value of the pertaining complex. Again, we find (Figure 8) that when $\mathcal{L}_2 = \mathcal{L}_1$, $\sigma = 1$ (the upper left corner of Figure 8). By increasing $\mathcal{L}_1$, at a given value of $\mathcal{L}_2$ (i.e., by keeping [^{2}L] constant and decreasing [^{1}L]), σ first increases and then decreases. This can be explained as follows: in the first step, the concentration of ^{1}L is not sufficient to form M^1L in significant proportions, but it is sufficient to decrease the lifetime of M at the consuming surface, i.e. to

increase the overall lability of the metal complexes. The flux is, thus, enhanced by increasing [^{1}L]. In the second step (i.e., after the maximum of σ), a further increase of [^{1}L] produces M^{1}L in significant and increasing proportions and an overall increase of lability of all complexes due to interfacial kinetic effect becomes less and less attainable, since the more labile complex M^{1}L becomes dominant. When $\mathscr{L}_1$ is maintained constant and $\mathscr{L}_2$ is increased, σ also increases first and then decreases. This reflects the fact that the flux enhancement results from the interplay between M^{1}L and M^{2}L, via M, at the interface: when the difference in lability indices of the two complexes is too large or too small, this interplay does not occur. So Figure 8 shows that, under the conditions used, an optimum ratio of $\mathscr{L}_1/\mathscr{L}_2 \approx 1000$ is required to get a maximum value of σ.

5. Conclusions

The present results show that the RLA, expressed in terms of composite reaction layers for solutions containing mixtures of ligands, is very useful for computation of metal fluxes at consuming interfaces. Furthermore, it provides a mechanistic level of understanding of the details of physicochemical processes taking place at the interface. The composite and equivalent reaction layer thicknesses, deduced in the RLA, clearly result from the interplay between all the complexes at the interface. They are validated quantitatively by the concentration profiles rigorously computed by numerical simulation. In particular, the RLA enables precise predictions to be made on the conditions of flux enhancement in two-ligand systems, i.e. under conditions where the interplay of complexes is very large. It has been shown that the flux enhancement depends on the relative labilities of the two complexes and their dynamic degrees of complexation.

It must be stressed that interplay between complexes at consuming interfaces may lead not only to flux enhancement of the less labile complex, when the concentration of ligand forming labile complexes is increased, but also to a decrease in flux of the more labile complex,[27] by increasing the concentration of ligand forming the less labile complex. This latter effect, however, is observable only when the two complexes are in similar proportions, i.e., the interfacial decrease of lability of the more labile complex is often masked by a simultaneous significant decrease of its proportion in the bulk solution. Overall, the impact of ligand mixtures on the dynamic speciation of the metal complex system is involved. The establishment of more quantitative relationships, e.g., between signals furnished by flux-based sensors and bio-uptake fluxes in mixed ligand media, must consider the potential interplay of species as detailed herein. In particular, when interpreting experimental flux measurements in unknown complicated media, it is difficult to assess the possible role of flux enhancement by a ligand forming labile complexes in very minor proportions. Extrapolating these results to other media, which do not contain this ligand and the corresponding complexes, may then lead to erroneous conclusions. Interpreting the experimental data by comparison with dynamic modeling may be very helpful in that respect.

Acknowledgment. This work was performed within the ECODIS project, funded by the European Commission's sixth framework program, subpriority 6.3 'Global Change and Ecosystems' under contract 518043.

Appendix

Definitions and Symbols

Definitions of Reaction Layer Thicknesses

μ	$(D_M/k_a[L])^{1/2}$, conventional expression of the reaction layer thickness, valid for a solution with one ligand, forming a strong complex ML with $D_{ML} \approx D_M$
λ	$(D_M/(k_a[L] + k_d/\varepsilon))^{1/2}$, general expression of the reaction layer thickness for a solution containing one ligand
$\bar{\lambda}$	composite reaction layer thickness, for a given complex in the presence of several other ligands, under conditions of semi-infinite diffusion (time-dependent diffusion layer thickness not imposed by geometric or hydrodynamic conditions)
${}^c\bar{\lambda}$	effective composite reaction layer thickness, as above, but under conditions where the diffusion layer thickness is imposed by external conditions and independent of time
$\tilde{\lambda}$	(fictitious) equivalent reaction layer thickness representative of the kinetics of the whole of the metal complexes in a mixture of ligands

List of Symbols

D_M	diffusion coefficient of free metal ion
J_t	total metal flux
J_{lab}	maximum metal flux when all the complexes are fully labile
J_t^0	sum of the separate fluxes of M, M^{1}L, and M^{2}L in the absence of the others
k_a	association rate constant of the reaction M + L $\rightleftharpoons$ ML
k_d	dissociation rate constant of ML
K	equilibrium constant of the reaction M + L $\rightleftharpoons$ ML
L	ligand
$\mathscr{L}$	lability index of the complex ML
ML	metal complex
α_j'	dynamic degree of complexation
ε	normalized diffusion coefficient of complex ML
σ	(J_t/J_t^0), the flux enhancement factor
δ	diffusion layer thickness

Supporting Information Available: Derivation of the conditions to obtain the flux enhancement in a solution containing two ligands, as well as the parameter values and species distribution used to compute the metal flux in the system Cu(II)-NTA−*N*-(2-carboxyphenyl)glycine. This material is available free of charge via the Internet at http://pubs.acs.org.

References and Notes

(1) *Metal Speciation and Bioavailability in Aquatic Systems*; IUPAC Series on Analytical and Physical Chemistry of Environmental Systems; Tessier, A., Turner, D., Eds.; John Wiley & Sons: Chichester, U.K., 1995; Vol 3.

(2) Morel, F. M. M.; Hering, J. G. *Principles and Applications of Aquatic Chemistry*; Wiley-Interscience: New York, 1983.

(3) Wilkinson, K. J.; Buffle, J. In *Physicochemical Kinetics and Transport at Biointerfaces*; IUPAC Series on Analytical and Physical Chemistry of Environmental Systems; van Leeuwen, H. P., Koester, W. Eds.; John Wiley & Sons: Chichester, U.K., 2004; Vol 9, pp 445−533.

(4) Playle, R. C. *Sci. Total Environ.* **1998**, *219*, 147.

(5) Campbell, P. G. C. In *Metal Speciation and Bioavailability in Aquatic Systems*; IUPAC Series on Analytical and Physical Chemistry of Environmental Systems; Tessier, A., Turner, D. R. Eds.; John Wiley & Sons: Chichester, U.K., 1995; Vol 3, pp 45−102.

(6) Sunda, W. G.; Huntsman, S. A. *Limnol. Oceanogr.* **2000**, *45*, 1501.
(7) Fortin, C.; Campbell, P. G. C. *Environ. Toxicol. Chem.* **2000**, *19*, 2769.
(8) Sunda, W. G.; Huntsman, S. A. *Limnol. Oceanogr.* **1995**, *40*, 1404.
(9) Sunda, W. G.; Huntsman, S. A. *Limnol. Oceanogr.* **1985**, *30*, 71.
(10) van Leeuwen, H. P.; Town, R. M.; Buffle, J.; Cleven, R. F. M.; Davison, W.; Puy, J.; Riemsdijk, W. H.; Sigg, L. *Environ. Sci. Technol.* **2005**, *39*, 8545.
(11) van Leeuwen, H. P.; Galceran, J. In *Physicochemical Kinetics and Transport at Biointerfaces*; IUPAC Series on Analytical and Physical Chemistry of Environmental Systems; van Leeuwen, H. P., Koester, W., Eds.; John Wiley & Sons: Chichester, U.K., 2004; Vol 9, pp 113−146.
(12) Galceran, J.; Puy, J.; Salvador, J.; Cecilia, J.; Mas, F.; Garces, J. L. *Phys. Chem. Chem. Phys.* **2003**, *5*, 5091.
(13) Alemani, D.; Chopard, B.; Galceran, J.; Buffle, J. *Phys. Chem. Chem. Phys.* **2005**, *7*, 3331.
(14) Alemani, D.; Chopard, B.; Galceran, J.; Buffle, J. *Phys. Chem. Chem. Phys.* **2006**, *8*, 4119.
(15) Zhang, Z.; Buffle, J. *J. Phys. Chem. A* , **2009**, *113*, 6562.
(16) Heyrovský, J.; Kuta, J. *Principles of Polarography*; Academic Press: New York, 1966.
(17) Brdička, R.; Wiesner, K. *Collect. Czech. Chem. Commun.* **1947**, *12*, 39.
(18) Brdička, R.; Wiesner, K. *Collect. Czech. Chem. Commun.* **1947**, *12*, 138.
(19) Koutecký, J.; Brdička, R. *Collect. Czech. Chem. Commun.* **1947**, *12*, 337.
(20) Koutecký, J. *Chem. Listy* **1953**, *47*, 323.
(21) Koutecký, J. *Collect. Czech. Chem. Commun.* **1953**, *18*, 597.
(22) van Leeuwen, H. P.; Puy, J.; Galceran, J.; Cecília, J. *J. Electroanal. Chem.* **2002**, *526*, 10.
(23) Buffle, J.; Startchev, K.; Galceran, J. *Phys. Chem. Chem. Phys.* **2007**, *9*, 2844.
(24) Zhang, Z.; Buffle, J.; van Leeuwen, H. P. *Langmuir* **2007**, *23*, 5216–5226.
(25) Alemani, D.; Buffle, J.; Zhang, Z.; Galceran, J.; Chopard, B. *Environ. Sci. Technol.* **2008**, *42*, 2021.
(26) Zhang, Z.; Buffle, J.; Startchev, K.; Alemani, D. *Environ. Chem.* **2008**, *5*, 204.
(27) Salvador, J.; Garcés, J. L.; Companys, E.; Cecilia, J.; Calceran, J.; Puy, J.; Town, R. M. *J. Phys. Chem. A* **2007**, *111*, 4304.

JP8114308